PHYSICAL REVIEW B VOLUME 45, NUMBER 17 1 MAY 1992-I

# Disorder and staging in iodine-doped polyacetylene

M. J. Winokur and J. Maron
*Department of Physics, University of Wisconsin, Madison, Wisconsin 53706*

Yong Cao and A. J. Heeger
*Department of Physics, University of California, Santa Barbara, California 93105*
(Received 2 August 1991)

Iodine doping of highly oriented *trans*-polyacetylene films has been studied using *in situ* x-ray diffraction of vapor- and solution-doped samples. In either case the initial doping transition is marked by coexistence of undoped polymer and that of an intermediate doped phase. At higher dopant concentrations the samples undergo additional structural evolution. Structure-factor calculations of suggestive models, in comparison to the equatorial profiles, indicate that the stepwise formation of well-ordered structural phases (i.e., staging) does not occur. An alternative model of the doping process is proposed whereby dopant uptake occurs in two distinguishable steps. Initially, a systematic "disordered" packing of quasi-one-dimensional iodine columns forms within the polymer host matrix, and, thereafter, the doping process is dominated by intercalation of unoccupied galleries to form layered iodine sheets.

## I. INTRODUCTION

Polyacetylene (PA) and its doped derivatives are among the most heavily studied of the highly conjugated polymers.[1] Of these, iodine-doped polyacetylene still receives considerable attention due to the relative ease of doping[2] and the extraordinarily high conductivities that are obtainable with improved synthesis routes.[3,4] As such, a detailed understanding of these particular doped phase structures seems especially important. Unfortunately, dopant-ion diffusion into the polymer host matrix by this moderately large molecular species effects a disruption of the basic polymer packing and consequently an appreciable loss of diffraction information.

In spite of this complication, considerable effort has been made toward interpreting the diffraction data that are available.[5–10] There are clear analogies to the structural phases of alkali-metal-doped PA[11] for iodine doping is also dominated by the formation of linear polyiodide-ion arrays that lie parallel to the polymer chains. Analysis of the equatorial scattering (perpendicular to the polymer chain axis) in these iodine-doped samples has produced an idealized model in which there is a systematic evolution of structure through a stepwise sequence of ordered arrangements by these one-dimensional iodine arrays within the polymer matrix.[8] This progression has been likened to the process of staging which is often observed in quasi-two-dimensional layered materials (e.g., graphite intercalation compounds[12]). In addition to direct structural observations, recent *in situ* transport measurements[4] have identified resistance anomalies during dopant uptake which have been interpreted in the context of this staging model.

In this communication we present results and analysis of x-ray-diffraction data obtained during *in situ* vapor and solvent doping studies of stretch-oriented PA. These results indicate that there are important aspects of doping process which have not been fully addressed in these prior structural studies. We find that while it is possible to achieve nearly complete "homogeneous" macroscopic doping of the polymer crystallites, a systematic microscopic disorder within the individual crystallites is always present. Hence the tendency to yield well-defined, high-symmetry structures appears to be strongly tempered by a propensity to form a disordered "mixed-stage" structure that maintains a nearly triangular nesting of the polymer chains. The iodine doping process appears to proceed through a two-step process with the dopant initially forming a structure in which the linear channels are surrounded by six polymer chains. Subsequent doping requires dopant insertion into the host matrix via a layer-by-layer process. Furthermore, these results also suggest that the polyiodide ions ($I_3^-$,$I_5^-$, etc.), which fill the one-dimensional channels, may be measurably tilted with respect to the polymer chain axis direction.

## II. EXPERIMENTAL DETAILS

The polyacetylene films employed in this experiment were synthesized using a modified Shirakawa process,[13] then stretch oriented to final draw ratios approaching 15:1 and finally isomerized to an all-*trans* conformation by thermal annealing at 160 °C for ca. 1 h. As is true for all PA films, fibrillar[14] or lamellar,[15] these films were polycrystalline in nature with small polymer crystallites embedded within less ordered polymer regions. Overall, the mosaic spread (the angular *c*-axis or chain axis distribution of crystallites about the draw direction) was less than 10° and the equatorial and chain-axis coherence lengths were typically ~80 and ~150 Å, respectively. In addition to the polymer host, thin nickel wire was comounted with the samples so that a direct estimate of the dopant concentration could be obtained by recording changes in the scattering intensity of the nickel (111) reflection.

The *in situ* vapor cell utilized for this study was a two-

 

zone glass and stainless-steel assembly fitted with 5-$\mu$m-thick mica windows that contributed no parasitic diffuse scattering to the diffraction profiles. After mounting in the diffractometer and opening an intervening valve, the $\sim$60-$\mu$m-thick PA films (two 30-$\mu$m-layers) could be monitored throughout the entire doping process. Thus any subtle sample-dependent variations were isolated. The use of vapor doping also avoided the presence of solvent and so greatly simplified the background subtraction. The only difficulties associated with this configuration were the need to include a partial pressure of Ar gas within the doping cell and the presence of a large iodine source to PA spacing ($\sim$10 cm). As a result of these two factors, onset of initial doping required at least 24 h and complete vapor doping at room temperature necessitated a minimum of 24 additional hours.

For solvent doping of the PA films a second, again mica-windowed, cell was employed through which solvent (typically heptane saturated with iodine) could be flowed intermittently. Solvent contributions to the diffraction profiles were minimized by limiting the total polymer-solvent path to less than 100 $\mu$m. Since the cell solvent volume was minimal (less than 0.1 cm$^3$), the polymer host could be fully doped only by introducing additional solvent at selected intervals. For the iodine-saturated heptane solutions, a minimum of three refills over the course of 12 h were necessary to achieve maximal iodine dopant concentrations. This flow cell also enabled doped samples to be partially undoped by refilling the cell with pure solvent after complete doping.

The x-ray-diffraction data were obtained using two different experimental setups which were attached to two separate ports of a 15-kW x-ray generator equipped with a copper anode ($\lambda$=1.542 Å). The first was a 4-circle diffractometer fitted with a linear silicon-diode array detector and has been described in greater detail elsewhere.[16] The second detector was a powder diffractometer equipped with an elastically bent LiF monochromator and a wire proportional detector which subtended a $2\theta$ angle of 120°. Equatorial profiles, which probe the structure perpendicular to the polymer chain axis, were acquired continuously during both vapor and solvent doping trials. At chosen intervals, the nonequatorial scattering was also examined. Structure factor calculations of the equatorial ($hk0$) intensities were performed using standard procedures[17] that included typical crystallographic factors (e.g., atomic scattering form factors[18]). Since the diffraction data contained only broad features, direct comparisons to the experimental data were attempted only after a convolution of the many Bragg reflections with a broad Lorentzian profile that represented a combined instrumental and sample ($\sim$40 Å) resolution function.

## III. EXPERIMENTAL RESULTS AND MODELING

Figure 1 displays a progression of equatorial ($hk0$) scattering profiles obtained during dopant uptake for a vapor-doped sample (after scaling the individual spectra to account for attenuation arising from iodine uptake). The iodine dopant concentration increases from bottom to top. For this sample the doping transition was accompanied by net 40% reduction in the transmitted intensities or, equivalently, an estimated maximum iodine concentration of $y \approx 0.10$ [using a compositional formula $(CH)I_y$]. In addition to the polymer contributions, the diffraction profiles also contain a smooth, monotonically decreasing background as a result of air scatter.

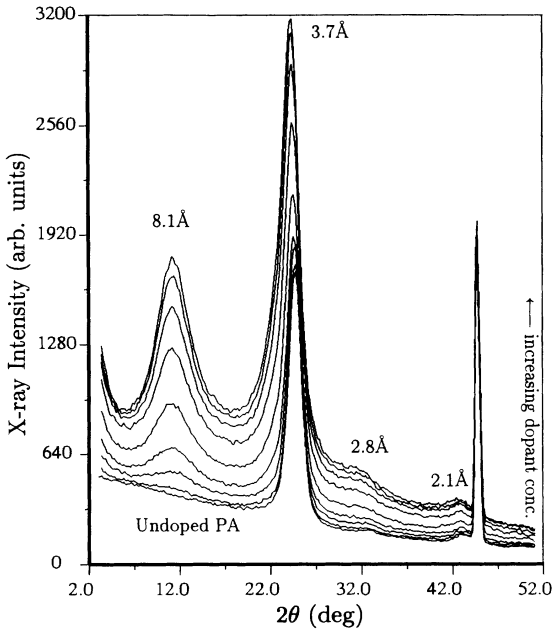


FIG. 1. Experimental data for equatorial ($hk0$) scattering during the vapor-doping transition of PA. Note the sharp feature near $2\theta$=45° is the Ni (111) reflection.

Vapor doping is most consistent with a two-phase coexistence of undoped polymer and that of a moderately doped phase. Throughout the entire doping process the scattering contribution by this doped phase to the ($hk0$) diffraction profiles smoothly increases while the proportion of undoped material gradually diminishes. If the top scan in Fig. 1 is considered to be representative of a completely doped sample (with $y \approx 0.10$), then all intermediate scans are well modeled by a simple linear superposition of $x$ and $1-x$ fractions of the undoped (bottom) and fully doped (top) diffraction scans, respectively. In particular, the line shape of the scattering intensity for the composite scattering peak in the vicinity of $2\theta$=24° is always accurately reproduced. Thus the effective proportion of iodine-doped PA is estimated to be in excess of 90%. Throughout this doping process there are no detected changes in the doped-phase diffraction profiles except for a proportionately more rapid rise in the scattering intensity at $2\theta$ angles of less than 4° during the initial scans. This effect at small angles is indicative of an inhomogeneous distribution of doped regions within the pristine polymer. The direct observation of a two-phase coexistence is also consistent with spin-susceptibility measurements which find that iodine doping is accompanied by an immediate appearance of metallic-like behavior.[19]

The most pronounced additional scattering features in the fully doped profile (Fig. 1 at the top) are the peaks centered about $2\theta$ positions of 10.9°, 24.1°, 31.5°, and 42.5° or, equivalently, $d$-spacings of 8.1, 3.7, 2.8, and 2.1 Å, respectively. A longer time equatorial scan (not shown) reveals a final weak scattering peak centered at 50.1° (or 1.8 Å). In addition to these features, there is a dramatic increase in the scattering intensity at all equatorial $2\theta$ positions. This scattering has been nominally identified previously as resulting from a disordered distribution of the iodine atoms within the host matrix.[6] Although these data are similar to equatorial profiles obtained by Murthy *et al.*[6] and Pouget *et al.*,[9] it is important to note than the 3.7-Å peak is always measurably *narrower* than the intense low-angle reflection. Furthermore there is a pronounced shoulder on the low-angle side this comparatively narrow peak and significant asymmetry in the line shape of the broader peak centered at 10.9°.

For the solution-doped PA sample, shown in Fig. 2 after again correcting for absorption effects of the iodine, there is an equivalent initial structural progression with coexistence of the undoped polymer and an iodine-doped phase whose scattering profile is essentially identical to that observed during the vapor-doping transition. In particular, the profile marked with an arrow in Fig. 2 compared favorably to the final vapor-doping equatorial scan in Fig. 1 (at the top). While the vapor-doped sample was limited to a dopant level of $y \approx 0.10$, continued dopant uptake could be observed in solution-doped samples and

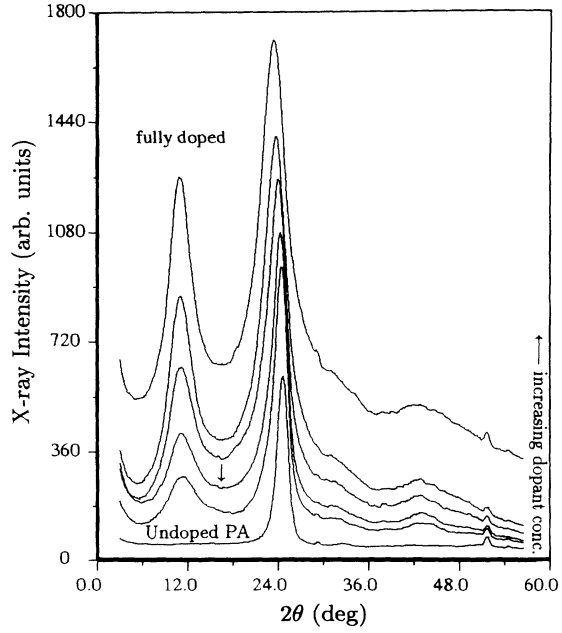


FIG. 2. Experimental data for equatorial ($hk0$) scattering (exclusive of solvent contributions) during solution-doping of PA. The scan marked by an arrow is comparable in both dopant concentration and profile to the top scan in Fig. 1. Note that the top scan in this figure has been translated upward for clarity and also note that any weak shoulders or sharp features are detector artifacts.

this polyacetylene film saturated at an estimated dopant concentration of $y \approx 0.25$. The most interesting aspect at this latter portion of the doping process is that the position of the 8.1-Å reflection, centered at $2\theta = 10.9°$, remains unchanged throughout while it narrows only slightly at the heaviest dopant levels. In contrast the scattering feature formerly at 24.1° appears to shift to lower angle (to 23.6°) and broaden significantly. The iodine-saturated scan, shown at top in Fig. 2, is also similar to equatorial profiles obtained by other studies.[5,8]

Undoping of a saturated solution-doped sample, by the addition of pure solvent to the flow cell, effected only a partial undoping. Ultimately a final iodine concentration of $y \approx 0.10$ was achieved with an equatorial scattering profile similar to that seen during dopant uptake (as indicated by the arrow in Fig. 2). Attempts to dedope a vapor-doped sample, by thermal heating, caused changes in the diffraction spectra suggestive of decomposition. Gradual variations in the diffraction profiles due to a slow loss of dopant were not investigated.[8]

The excellent statistics of these data sets allows for detailed comparisons with a variety of possible structural models. In particular, the topmost scattering profile in Fig. 1, with a nominal $y \approx 0.10$ iodine concentration, has been studied. Integrated peak intensities from this profile compare favorably to those obtained in structure-factor calculations using the previously proposed UPUP[8,20] oblique unit cell depicted in Fig. 3(a). However, as can be seen in Fig. 4 at the bottom, direct comparison to the actual scattering data is not entirely satisfactory for the peak positions of the most intense scattering features are not well represented and there are many pronounced weaker features in the calculated profiles which are not present in the experimental data. Simple variations in these lattice parameters do not yield improved fits.

Interestingly, we note that the reflections at 24.1°, 42.6°, and 50.1° have wave vector ratios which are very close to the nominal $1:\sqrt{3}:2$ ratio appropriate for a triangular lattice. Thus, the nearly triangle average packing by the polymer chains which exists in the pristine PA host seems to be a recurring theme even after the considerable distorting influences of the iodine dopant. A similar response is observed during the doping-induced transformations by the smallest of alkali-metal dopants in which quasi-one-dimensional alkali-metal channels are formed by three neighboring PA chains,[21,22] but for iodine-doped samples a threefold column structure is clearly unphysical. By invoking a triangular lattice of the polymer chains with a 4.3-Å repeat, the positions of these three reflections can be reproduced. In order to systematically introduce the iodine dopant, individual PA chains are replaced by iodine column so that various "superlattice" structures are generated. These structures are simply representative of possible high-symmetry base structures and do not accurately describe the process of dopant-ion insertion into the host matrix. These models are depicted in panels (b) through (d) of Fig. 3. Each model can be interpreted as having a sixfold channel structure with a $2\times2$, a $\sqrt{7}\times\sqrt{7}$, or a $\sqrt{7}\times2$ packing, respectively, of the dopant channels. Adjustments to the PA angular orientation within the equatorial plane gen-

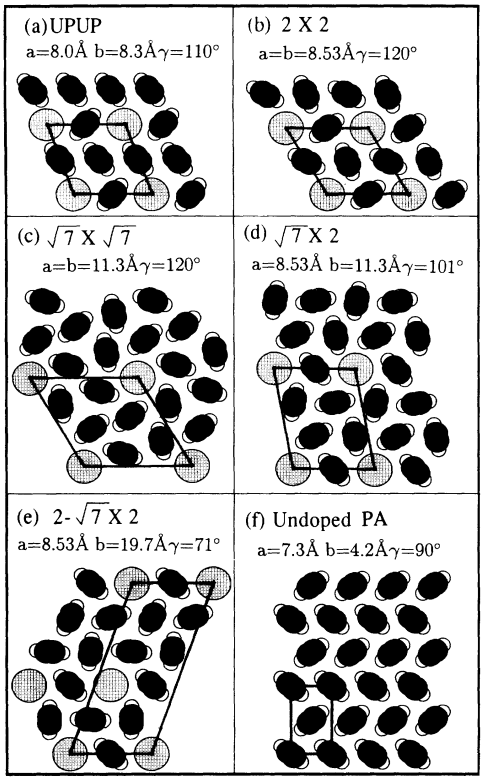


FIG. 3. Projected equatorial structures (perpendicular to the $c$ axis) for (a) the proposed intermediate iodine-doped PA model (UPUP) of Ref. 8 ($y=0.13$); (b) a $2\times2$ ($y=0.13$); (c) $2\times\sqrt{7}$ ($y=0.18$); (d) $\sqrt{7}\times\sqrt{7}$ ($y=0.06$); (e) $2-\sqrt{7}\times2$ ($y=0.10$); (f) undoped *trans*- PA. Note that black, white, and hatched circles represent carbon, hydrogen, and iodine atoms, respectively.

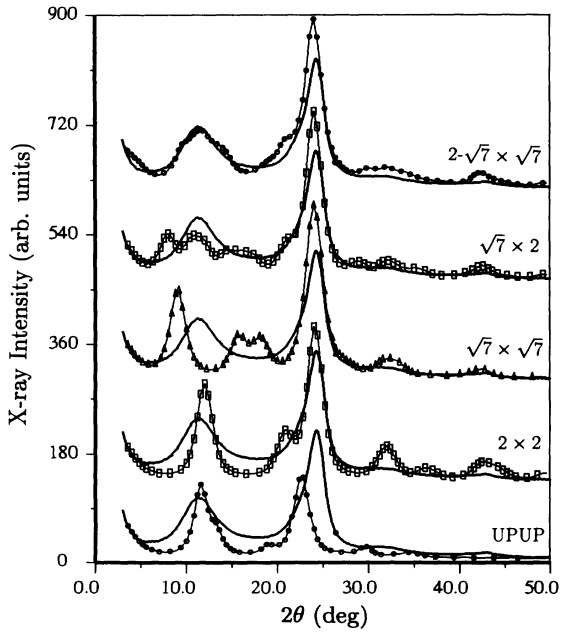


FIG. 4. Comparison of the experimental ($hk0$) data (solid lines) for the fully vapor-doped PA sample (top scan in Fig. 1) as compared to structure factors (various symbols connected by lines) calculated for the respective models depicted in Fig. 3.

erate only modest changes in relative peak intensities. In general these base structures, with or without simple distortions and with the average iodine intrachannel spacing[8] fixed at 3.1 Å, provide calculated structure factor profiles which are unsatisfactory either individually or as combined linear superpositions. A more complicated model incorporating a $2-\sqrt{7}\times2$ organization of the dopant channels [Fig. 3(e)] gives a somewhat better calculated structure factor (Fig. 4 at the top). Presently there does not appear to be a simple structural model which can accurately follow the experimentally observed intensity variations of this (or any other) equatorial scattering profile.

Before introducing a more complicated model, it is instructive to discuss the nonequatorial data. By employing a sequence of radial $\theta-2\theta$ scans with the polymer chain axis at varying degrees of inclination to the scattering plane of the detector, the nonequatorial data can be acquired and a map of constant scattering intensity contours can be reconstructed. These data are displayed in Fig. 5 and are again quite similar to diffractometer[8] and film[13] data reported in the literature. The most significant nonequatorial feature is the pronounced layer line (parallel to the equatorial plane) which is attributed to scattering by linear iodine-ion arrays whose average iodine atom spacing is 3.1 Å. We also note that there can be weak, but measurable, intensity modulations along this layer line indicative of slight interchannel correlations between neighboring iodine channels. Additional layer lines, with very weak intensities, are observed in the individual scans which make up this contour map. In addition to these layer lines, there is a diffuse scattering halo centered about $2\theta=20°$ and oriented in the equatorial

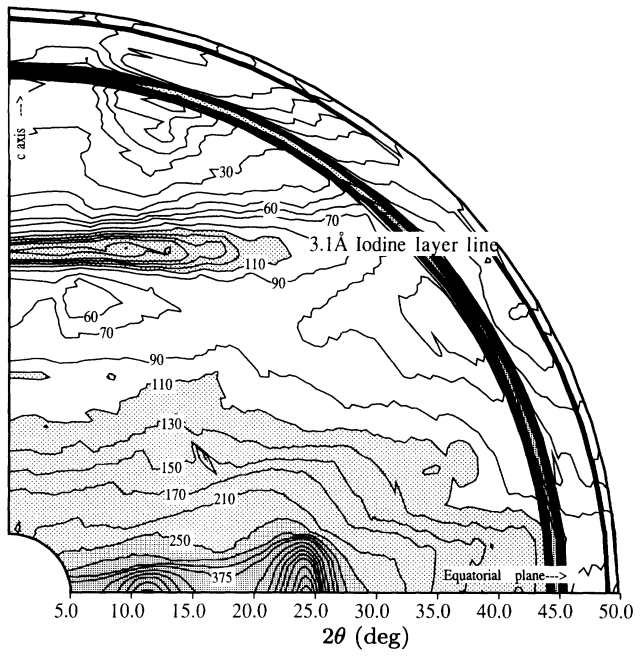


FIG. 5. Map of constant scattering intensity contours from the equatorial ($hk0$) plane to the $c$ axis (parallel to the polymer chain axis) for the fully vapor-doped sample ($y\approx0.10$) of Fig. 1. Note that the intense arcing feature at $2\theta\approx45°$ arises from scattering by Ni wire comounted with the PA sample.

plane. This scattering is seen to have both a strong equatorial component and a less pronounced nonequatorial component. Since uniaxial stretching often preferentially aligns crystalline regions as opposed to the amorphous fractions,[23] a large proportion of this scattering background appears to originate from structural features contained within iodine-doped polymer crystallites as opposed to scattering by iodine-ions situated within amorphous fractions.

The presence of this scattering feature from "crystalline" regions of the host may imply an uneven filling of the iodine columns or, alternately, the presence of severe equatorial disorder. In light of the estimated 100-Å intrachannel coherence length for iodine ions which fill the columns (derived from the Scherrer formula

$$L=\frac{0.9\lambda}{\Delta 2\theta\cos\theta} \tag{1}$$

and determining $\Delta 2\theta$ from the leading edge of the 3.1-Å intense layer line acquired in a meridional scan), the latter process seems more likely. If a random uniaxial sequencing of the basic $2\times 2$ and the doubly degenerate $\sqrt{7}\times 2$ structure is generated (as seen in the Fig. 6 inset), then all essential features characteristic to the scattering data of the intermediate doped phase can be faithfully reproduced. In particular, the rather narrow 24.1° peak width is accurately depicted as well as a large part of the scattering intensity that is observed over the entire equatorial scattering profile. The broad peak at $2\theta=10.9°$ is simply representative of an average 8.1-Å distancing between adjacent layers of partially iodine occupied rows. The low-angle shoulder of the 24.1° peak then becomes the second-order reflection of this fundamental spacing. Its comparatively weak intensity, as compared to first- and third-order reflections, implies that there must be equatorial displacements of the iodine chains within the one-dimensional columns with a distribution somewhat different than that assumed by the introduction of a simple exponential Debye temperature factor. Hence we conclude that the iodine atoms do not form perfectly linear arrays, but that either tilting or a staggering of the iodide ions is present.[24] If the intrachannel iodine concentration is arbitrarily varied, the best fits occur at dopant concentrations near 10% mole weight of iodine. This composition compares very favorably with compositions determined by x-ray absorption (in this sample) or weight uptake measurements of similarly doped samples analyzed elsewhere.[8,10,13] Because of the intrinsic disorder associated with this model, an accurate estimate of the actual polyacetylene setting angles (i.e., rotation of the polymer chain about the chain axis) is difficult to establish.

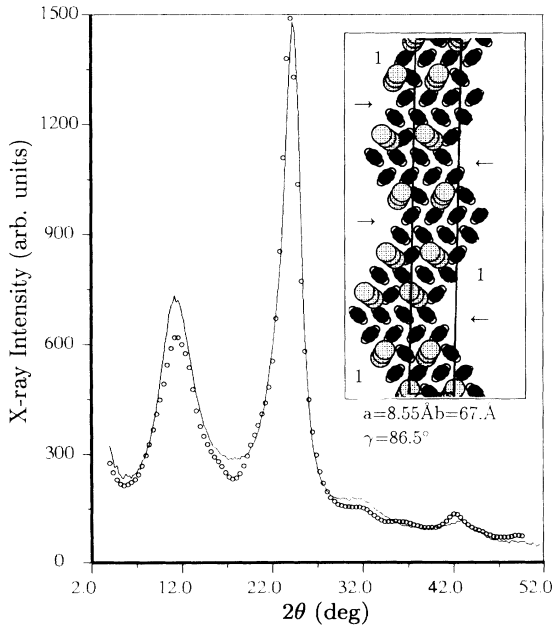


FIG. 6. Experimental ($hk0$) data (solid line, comparable to the top scan in Fig. 1 without air scatter) for a fully vapor-doped PA sample as compared to the calculated structure factor (circles) from the representative intermediate doping model (containing two unit cells side by side) shown in the inset with $y=0.10$. The arrows point to residual polyacetylene double layers and the numbers identify single PA layers.

The continued doping evolution toward saturation can also be easily accommodated within the context of this proposed intermediate doping structure. Nominally there are two possibilities which must be considered, either the iodine-ion density within a dopant column is increased or the actual number of dopant channels increases (or both). For all dopant levels examined by meridional diffractometer scans, in which the diffraction vector is maintained parallel to the polymer $c$ axis, the average iodine repeat remained fixed at 3.1 Å and the peak intensity either increased or decreased smoothly. This indicates that the average iodine spacing is compositionally independent and that only by formation of additional structurally similar iodine arrays can further dopant uptake be readily achieved. Considering the base structural characteristics of the proposed intermediate dopant-level model, it appears unlikely that a dramatic secondary structural reorganization with the formation of additional sixfold channel structures would occur.

A straightforward solution is reached by directly introducing staggered iodine-ion layers between the remaining double layers of polyacetylene only chain. These layers are indicated by arrows in the inset of Fig. 6. A comparison of the structure factor calculation, assuming that each all-PA double-layer gallery becomes completely filled by iodine-ion arrays spaced every ~4.27 Å (see Fig. 7 inset), with the equatorial profile of the iodine saturated solution-doped polymer is displayed in Fig. 7. The overall fit is quite reasonable except for the appearance of an additional scattering feature centered near $2\theta=47°$. This peak primarily represents a superposition of scattering contributions from the fourth-order reflection of the average iodine layer-to-layer repeat and that from the second-order ~3.7 Å spacing of the PA chains. Selectively increasing the disorder may remove this feature.

In order to obtain the "best"-fit scattering profile for the intense peak centered at 23.6°, it was also necessary to include ~2.1 Å translational displacements of the

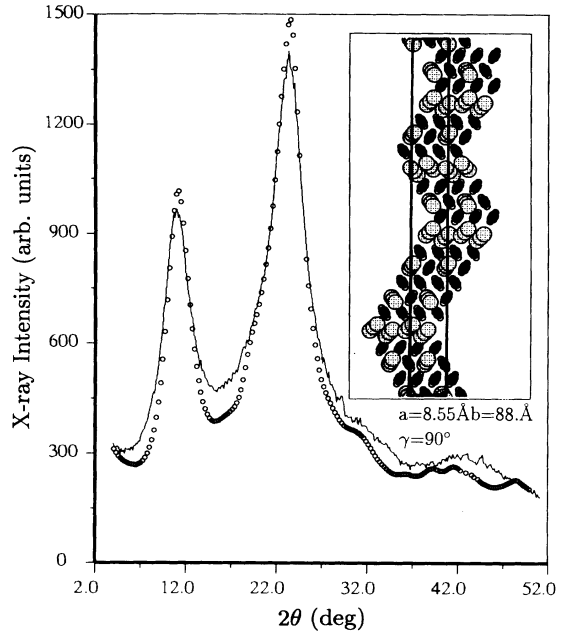


FIG. 7. Experimental ($hk0$) data (solid line, from the top scan in Fig. 2) for a fully solution-doped PA sample as compared to the calculated structure factor (circles) from the representative heavy doping model contained in the inset ($y=0.22$). Note that the inset contains two unit cells nested side by side.

guest-host matrix parallel to the **a** axis when introducing any all-iodine layers. The significant feature in this latter translation is that the triangular nesting of the polymer chains is thereby maintained across these iodine-only layers. Finite-size effects are still present in this model, as well as that of the intermediate dopant level, because there is modest sensitivity to the boundary conditions. The calculated structure factors are not overly sensitive to the actual positioning of the iodine channels within the all-iodine layers and hence the intralayer 4.27 Å spacing of the iodine columns in the depicted model is for visual simplicity. As can be seen in Fig. 8, an arbitrarily severe increase in the iodine ion array density, by some 50% within iodine-only layers, does alter the calculated equatorial profiles substantially although many basic features are still retained.

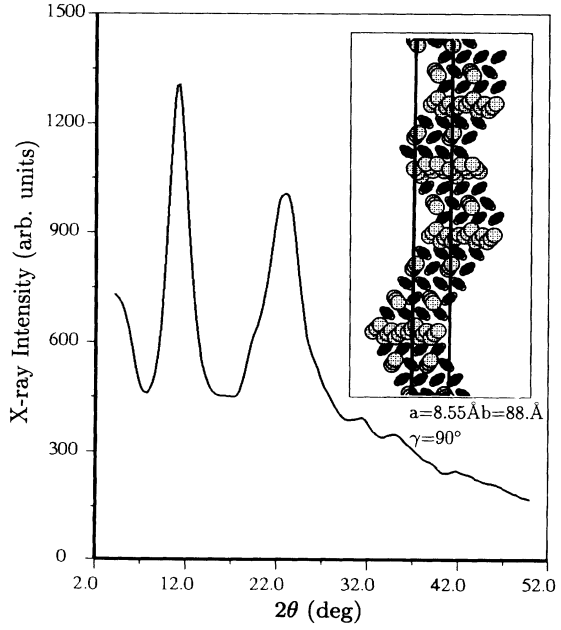


FIG. 8. Calculated structure factor from a structural model in which the iodine concentration has been artificially increased by 50% within all-iodine layers ($y=0.28$) as shown in the inset.

## IV. DISCUSSION AND CONCLUSIONS

While these aforementioned models can provide significantly improved fits to the experimental data, their overall uniqueness is an important issue. Since there are many possible degrees of freedom available, the specific details of the respective packings are of limited utility. It is likely that further structural modifications, with minimal or no physical significance, we can obtain even closer fits to the actual experimental data. However, the general features of the doping process, as indicated by comparisons of these models to the experimental data, should be essentially correct and thus enable a realistic account of the doping-induced structural progression within the polymer host. Previous models have required that partially iodine-filled layers are selectively replaced by all-iodine layers. This implies that drastic local polymer chain reorganizations must occur at each stage of the doping process.

Our proposed intermediate model, as seen in the inset of Fig. 6, still requires that the initial doping-induced transformation deviate strongly from that of the alkali dopants for the latter require only local polymer chain rotations and global expansion and/or contraction of the host matrix in order to accommodate dopant-ion diffusion.[25] In order to transform undoped PA [see Fig. 3(f)] into the alternating PA/*I*/PA/*I*/,..., layers of the intermediate structure, significant relative translational displacements of the polymer chains are essential. This therefore accounts for the appreciable loss in structural perfection of the composite compound. However once this structure forms, the sixfold channels are dimensionally stable and there are only minimal reductions in the crystalline order during additional dopant uptake. The absence of a clear periodicity between individual PA/*I*/PA/*I*/,..., layers in this intermediate stage also implies that a range of dopant concentrations and lattice spacings are potentially possible for differing PA samples and/or doping conditions. Interestingly, we find that PA samples which have been inadvertently exposed to oxidizing conditions do not readily achieve as high dopant concentrations.[26]

When only single and double all-polyacetylene layers remain, as indicated by the ones and arrows, respectively, in the inset of Fig. 6, continued dopant uptake does not (and cannot) induce further formation of sixfold channels. Thus, a second doping-induced structure prevails. This latter structure is associated with the stepwise insertion of all-iodine layers between any available PA double layers. It is probable that the discontinuity in the con-

ductivity measured *in situ*[4] is associated with a rapid increase in the formation of these all-iodine layers. Since there is a distribution of potential intermediate structures, there will be an even wider range in the dopant concentrations of the saturation structures.

For either dopant organization, sixfold channels or all-iodine layers, the average iodine $c$-axis spacing, parallel to the polymer chain axis, is found to be essentially identical. Because of the decreased PA chain to iodine column ratio that is necessary for all-iodine layer formation, an increase in the relative proportion of $I_5^-$ ions, as opposed to $I_3^-$, may be a compensating effect which reduces the effective concentration of negative charge within all-iodine layers. Further x-ray studies of the very weak nonequatorial scattering features may be able to observe structural evidence for this behavior. We note that examples of layered guest-host composites with high concentrations of negative charged ions within the dopant layer, such as low stage Br-intercalated graphites,[27] are well known.

Our studies also suggest that rapid undoping of the iodine saturated polyacetylene films is dominated by a sequential loss of these secondary all-iodine layers. In contrast to previous x-ray studies, we were unable to obtain equatorial diffraction profiles which yielded lattice $d$-spacings of $\sim 14$ Å.[8] Because their results were not obtained *in situ*, it seems likely that the appearance of this periodicity is intimately related to the environmental treatment of the polymer host during the undoping process.

Due to absence of well-defined stages during iodine doping, the two different modes of dopant uptake, sixfold columns, and all-iodine layers, should probably not be viewed as being mutually exclusive. It is likely that iodine-layer formation accompanies initial dopant uptake to some extent but at a much reduced rate as when compared with latter stages of the doping process. Although the limited structural information available leaves many important questions concerning the local polymer-guest structure unresolved, these *in situ* techniques have enabled a more comprehensive analysis of the doping process and realized an enhanced understanding of the overall structure and structural evolution.

## ACKNOWLEDGMENTS

The financial support by NSF DMR Grant No. DMR-8917530 (M.J.W.), by the University of Wisconsin (J.M.) and by the Electric Power Research Institute under EPRI-RP8007-9 (Y.C. and A.J.H.) is gratefully acknowledged.

[1]For a general review, see *Handbook of Conducting Polymers,* edited by T. Skotheim (Marcel Dekker, New York, 1986), Vols. 1 and 2.

[2]For the most recent International Conference on Synthetic Metals Proceedings, see Synth. Met. **41**, (1991).

[3]N. Basescu, Z.-X. Liu, D. Moses, A. J. Heeger, H. Naarmann, and N. Theophilou, Nature (London) **327**, 403 (1987).

[4]J. Tsukamoto, A. Takahashi, and K. Kawasaki, Jpn. J. Appl. Phys. **29**, 125 (1990).

[5]M. Monkenbusch, B. S. Morra, and G. Wegner, Makromol. Chem. Rapid Commun. **3**, 69 (1982).

[6]R. H. Baughman, N. S. Murthy, G. G. Miller, and L. W. Shacklette, J. Chem. Phys. **79**, 1065 (1983).

[7]S. Flandrois, C. Hauw, and B. Francois, J. Phys. (Paris) **44**, C3 (1983).

[8]N. S. Murthy, G. G. Miller, and R. H. Baughman, J. Chem. Phys. **89**, 2523 (1988).

[9]J. P. Pouget, J. C. Pouxviel, P. Robin, R. Comes, D. Begin, D. Billaud, A. Feldblum, H. W. Gibson, and A. J. Eptein, Mol. Cryst. Liq. Cryst. **117**, 75 (1985).

[10]P. Robin, J. P. Pouget, R. Comes, H. W. Gibson, and A. J. Epstein, Polymer **24**, 1558 (1983).

[11]R. H. Baughman, N. S. Murthy, and G. G. Miller, J. Chem. Phys. **79**, 515 (1983).

[12]*Intercalation in Layered Materials,* edited by M. S. Dresselhaus (Plenum, New York, 1986).

[13]Yong Cao, Paul Smith, and A. J. Heeger, Polymer **32**, 545 (1991).

[14]H. Shirakawa and S. Ikeda, J. Polym. Sci. **2**, 3 (1971).

[15]J. H. Edwards and W. J. Feast, Polymer **21**, 595 (1982).

[16]D. Chen, M. J. Winokur, M. Masse, and F. E. Karasz, Phys. Rev. B **41**, 6759 (1990).

[17]L. E. Alexander, *X-Ray Diffraction Methods in Polymer Science* (Wiley, Interscience, New York, 1969).

[18]*International Tables for X-Ray Crystallography* (Kynoch Press, Birmingham, 1974), Vol. IV.

[19]A. J. Epstein, H. Rommelmann, M. A. Druy, A. J. Heeger, and A. G. MacDiamid, Solid State Commun. **38**, 683 (1981).

[20]The UP designation refers to the presence of undoped (U) and partially doped (P) layers.

[21]M. J. Winokur, Y. B. Moon, A. J. Heeger, J. Barker, D. C. Bott, and H. Shirakawa, Phys. Rev. Lett. **35**, 2329 (1987).

[22]N. S. Murthy, L. W. Shacklette, and R. H. Baughman, Phys. Rev. B **40**, 12 550 (1989).

[23]I. M. Ward, *Structure and Properties of Oriented Polymers* (Applied Science, London, 1975).

[24]Both tilting and staggering produce a distribution which preferentially reduces even-order reflection intensities.

[25]P. A. Heiney, J. E. Fischer, D. Djurado, J. Ma, D. Chen, M. J. Winokur, N. Coustel, P. Bernier, and F. E. Karasz, Phys. Rev. B **44**, 2507 (1991).

[26]This seems the most likely explanation for the maximum $y \approx 0.10$ in our vapor-doped samples.

[27]A. Erbil, A. R. Kortan, and R. J. Birgeneau, Phys. Rev. B **28**, 6329 (1983).

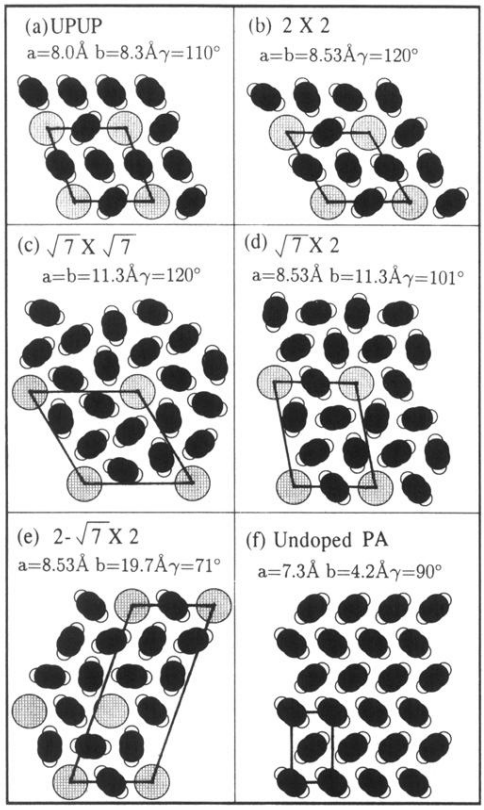


**FIG. 3. Projected equatorial structures (perpendicular to the *c* axis) for (a) the proposed intermediate iodine-doped PA model (UPUP) of Ref. 8 ($y=0.13$); (b) a $2\times2$ ($y=0.13$); (c) $2\times\sqrt{7}$ ($y=0.18$); (d) $\sqrt{7}\times\sqrt{7}$ ($y=0.06$); (e) $2-\sqrt{7}\times2$ ($y=0.10$); (f) undoped *trans*- PA. Note that black, white, and hatched circles represent carbon, hydrogen, and iodine atoms, respectively.**

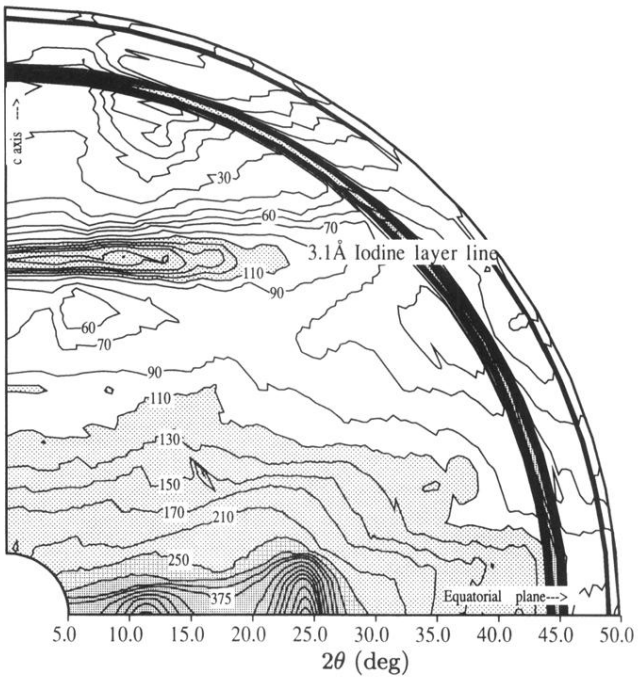


FIG. 5. Map of constant scattering intensity contours from the equatorial ($hk0$) plane to the $c$ axis (parallel to the polymer chain axis) for the fully vapor-doped sample ($y \approx 0.10$) of Fig. 1. Note that the intense arcing feature at $2\theta \approx 45°$ arises from scattering by Ni wire comounted with the PA sample.

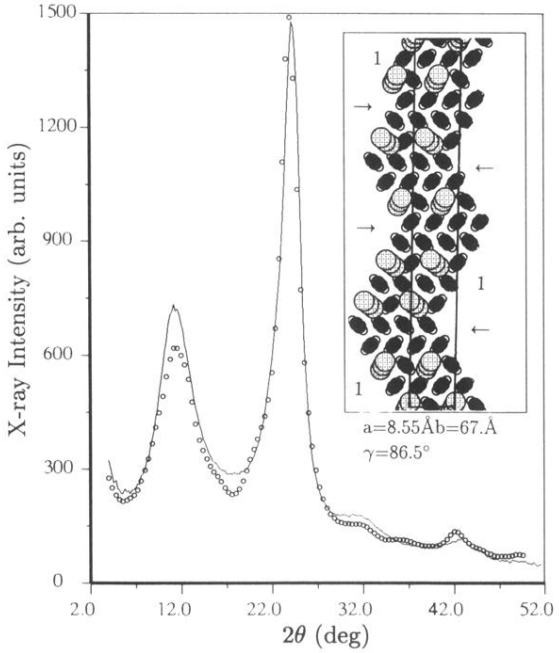


FIG. 6. Experimental ($hk0$) data (solid line, comparable to the top scan in Fig. 1 without air scatter) for a fully vapor-doped PA sample as compared to the calculated structure factor (circles) from the representative intermediate doping model (containing two unit cells side by side) shown in the inset with $y=0.10$. The arrows point to residual polyacetylene double layers and the numbers identify single PA layers.

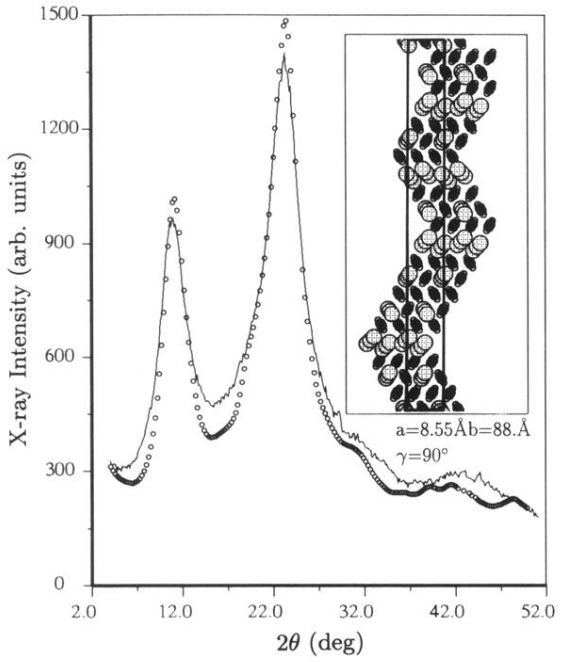


FIG. 7. Experimental ($hk0$) data (solid line, from the top scan in Fig. 2) for a fully solution-doped PA sample as compared to the calculated structure factor (circles) from the representative heavy doping model contained in the inset ($y=0.22$). Note that the inset contains two unit cells nested side by side.

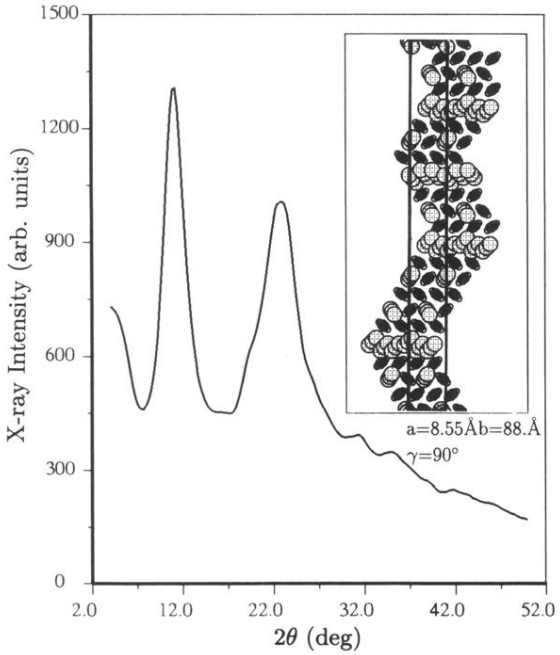


FIG. 8. Calculated structure factor from a structural model in which the iodine concentration has been artificially increased by 50% within all-iodine layers ($y=0.28$) as shown in the inset.